# Calcium action potentials in hair cells pattern auditory neuron activity before hearing onset

Nicolas X. Tritsch, Adrián Rodríguez-Contreras, Tom T.H. Crins, Han Chin Wang,
J. Gerard G. Borst & Dwight E. Bergles

# Supplementary Information

## Supplementary Methods

All experimental procedures used in this study were performed in strict accordance with protocols approved by the Animal Care and Use Committees at Erasmus MC and Johns Hopkins University.

***In vitro* SGN and IHC recordings.** Cochlear turns of postnatal day (P) 0–7 Sprague-Dawley rats were isolated in ice-cold, sterile-filtered HEPES-buffered ACSF containing (in mM): 130 NaCl, 2.5 KCl, 10 HEPES, 1 $NaH_2PO_4$, 1.3 $MgCl_2$, 2.5 $CaCl_2$, 11 D-glucose (290 $mmol.kg^{-1}$), pH 7.4, supplemented with 10 U/ml penicillin (Sigma). Explants were plated on Cell-Tak (BD Biosciences) coated glass coverslips and maintained for 1 to 7 days *in vitro* in F-12/DMEM (Invitrogen) containing 1% fetal bovine serum and 10 U/ml penicillin in a 37 °C, 5% $CO_2$ humidified incubator. Some experiments (**Fig. 2a–c**, and **Supplementary Fig. 2h–n**) were performed using cochlear turns acutely isolated from P4–9 rats, as described previously[1,2]. For recording, coverslips were continually superfused with bicarbonate-buffered ACSF composed of (in mM): 119 NaCl, 5 KCl, 1.3 $CaCl_2$, 1.3 $MgCl_2$, 1 $NaH_2PO_4$, 26.2 $NaHCO_3$, and 6 D-glucose (290 $mmol.kg^{-1}$), saturated with 95% $O_2$/5% $CO_2$, at 22–24 °C. Some experiments were performed with ACSF heated to 32–35 °C by passing it through a feedback-controlled in-line heater (Warner Instruments) prior to entering the chamber. Electrodes for loose-patch SGN recordings had a tip resistance of 0.7–1.5 MΩ when filled with HEPES-buffered ACSF and action potential waveforms were detected with patch resistances of 5–15 MΩ. Whole-cell current-clamp recordings from IHCs were obtained using 5–9 MΩ patch pipettes filled with internal solution composed of (in mM): 120 $KCH_3SO_3$, 20 HEPES, 10 EGTA, 1 $MgCl_2$, 2 $Na_2ATP$ and 0.2 NaGTP (290 $mmol.kg^{-1}$), pH 7.3. Paired IHC-SGN recordings were performed in cultured cochlear explants superfused with bicarbonate-buffered ACSF containing 2.5 mM KCl and 11 mM D-glucose. Most SGNs only contacted one IHC (see **Supplementary Fig. 4**); cells that received input from multiple IHCs were excluded from analysis. Currents and potentials were recorded with pClamp9 software using a Multiclamp 700A amplifier, low-pass filtered at 2–10 kHz, and digitized at 10–50 kHz with a Digidata 1322A analog-to-digital converter (MDS Analytical Technologies).

***In vivo* MNTB recordings.** Wistar rat pups (P0–8) were anesthetized with isoflurane (1.5%) delivered via a mouse ventilator. The MNTB was accessed using a ventral craniotomy as described previously[3]. Recordings were made at a depth of 300–400 μm from the pial surface using patch pipettes (5–8 MΩ) filled with artificial cerebrospinal fluid (ACSF) containing (in mM): 125 NaCl, 2.5 KCl, 1 $MgSO_4$, 2 $CaCl_2$, 1.25 $NaH_2PO_4$, 0.4 ascorbic acid, 3 *myo*-inositol, 2 pyruvic acid, 25 D-glucose, 25 $NaHCO_3$ (310 $mmol.kg^{-1}$), pH 7.4 when saturated with 95% $O_2$/5% $CO_2$, or intracellular solution containing (in mM): 126 K-gluconate, 20 KCl, 10 $Na_2$-phosphocreatine, 4 MgATP, 0.3 $Na_2GTP$, 0.5 EGTA and 10 HEPES (310 $mmol.kg^{-1}$), pH 7.2. Extracellular potentials were detected in the loose-patch configuration (10–50 MΩ). Potentials were recorded with pClamp9 software using an Axopatch 200B amplifier, filtered at 2–5 kHz and sampled at 20 kHz with a Digidata 1440A (MDS Analytical Technologies). Inclusion of Alexa Fluor 594 (0.012 %, Invitrogen) in pipette solutions allowed *post hoc* confirmation of extracellular recording sites within MNTB in paraformaldehyde-fixed brainstem sections (**Supplementary Fig. 5**). To test whether the burst pattern observed in the MNTB originated in the cochlea, the contralateral cochlea of P4–8 rat pups was ablated using a ventral approach ($n$ = 8). After opening the bulla and removing its contents, a hole in the ventral surface of the cochlea was made and the organ of Corti was disrupted with tweezers. In each case, prior to ablating the cochlea, we confirmed the location of the MNTB by recording from bursting units with complex waveforms and by post mortem histology. To confirm that silent units included principal cells, we stimulated the afferent fibers at the midline of ablated animals with 0.1 ms, 0.2 – 1 mA current pulses using a bipolar Tungsten electrode (0.1 MΩ impedance; tip separation 250 μm; MicroProbes for Life Science, Gaithersburg, MD).

***In vivo* CIC recordings.** Sprague-Dawley rat pups (P4–7) were anesthetized with either isoflurane (0.5–1.5%) or intraperitoneal injection of ketamine (15 μg/g) and xylazine (0.23 μg/g). After stabilizing the skull using a small custom-made metal plate and dental cement, a craniotomy was performed in the interparietal bone overlaying the inferior colliculus and filled with low melting point agarose (type IB, 1.5% in HEPES-buffered ACSF) to minimize brain motion. Multi-unit recordings were obtained at a depth of 200–1000 μm below the pia using glass electrodes (3–10 MΩ) filled with HEPES-buffered ACSF. Extracellular potentials were recorded with pClamp9 software using an Axopatch 1D amplifier, band-pass filtered at 5–5000 Hz and sampled at 20 kHz with a Digidata 1322A (MDS Analytical Technologies). For bilateral cochlear ablations the cochlea was accessed laterally following crude dissection of the bulla caudal to the pinna and removal of middle ear mesenchyme using fine forceps. After cauterizing the stapedial artery, the otic capsule was opened and the contents of the cochlea were entirely removed using vacuum-assisted suction. Complete bilateral ablation was verified after each experiment with cochlear dissections. The sham-operated group is composed of animals with unilateral or incomplete bilateral ablation. To minimize selection biases, recordings in control

and ablated animals were standardized for penetration steps (100-150 μm) and time allotted per recording site (>3 min).

**Data Analysis.** Data were analyzed off-line using Clampfit 9.2 (MDS Analytical Technologies), Origin (Microcal Software) or custom procedures written in the NeuroMatic environment (version 2.0, kindly provided by Dr. J. Rothman, University College London) within Igor Pro 6 (WaveMetrics). Data are expressed as mean ± standard error of the mean (s.e.m.). Statistical tests are noted in text (significance: $\alpha < 0.05$).

*Burst identification and separation*. Extracellular action potentials were identified by an amplitude threshold criterion. Cells were operationally classified as bursting if inter-spike intervals (ISIs) ranged from values <50 ms to values >1 s. A common measure of ISI variability within a given recording is the coefficient of variation ($CV_{ISI}$), defined as the ratio of the ISI standard deviation and ISI mean. Randomly-firing units have $CV_{ISI}$ values close to 1. On the other hand, non-stochastic or irregularly-firing units typically display $CV_{ISI}$ values greater than 1; the $CV_{ISI}$ of all 'bursting' MNTB units in this study (4.0 ± 0.2, $n$ = 50) was significantly larger than the $CV_{ISI}$ of the 'non-bursting' group (1.2 ± 0.3, $n$ = 18, $P < 0.001$, two-sample t-test). Similarly, $CV_{ISI}$ of all bursting IC units averaged 3.2 ± 0.2 ($n$ = 21). To objectively identify peaks in SGN and MNTB ISI histograms we obtained two boundary values – one in the 5–50 ms range (to separate first and second peaks) and one in the 1–10 s range (to separate the second and third peaks) – by calculating for each spike $CV_b$, defined as:

$$C_{Vb} = \frac{2\left|\Delta t_{i+j} - \Delta t_i\right|}{\Delta t_{i+j} + \Delta t_i}$$

where $\Delta t_i$ is the $i$'th ISI, with $i$=1, 2,… and $\Delta t_{i+j}$ is the next interval in the same interval class, with $j$=1, 2, … For the calculation of $CV_b$ each ISI was paired (if possible) with the next ISI belonging to the same interval class. To find the matching interval, intervals belonging to a class with smaller intervals are skipped. If an interval belonging to a class with a larger interval came before the next same-class interval, the value for $CV_b$ is not obtained for that spike. The mean of all obtained $CV_b$ values will be a measure for the overall within-class homogeneity. Bursts were separated by finding the two boundary values for which mean $CV_b$ was minimal. Lower boundaries were on average 31.8 ± 2.6 ms (range: 8.1–50.3 ms), 38.5 ± 1.5 ms (range: 14.8–49.7 ms) and 46.3 ± 0.9 ms (range: 34.4–49.7 ms) for *in vitro* SGN ($n$ = 35 room and physiological temperature), *in vivo* MNTB ($n$ = 50) and *in vivo* CIC ($n$ = 21) recordings, respectively, and higher boundaries were 2.0 ± 0.2 s (range: 1.0–5.2 s), 2.2 ± 0.2 s (range: 1.0–7.6 s) and 3.1 ± 0.6 s (range: 1.0–10.1 s), respectively. For comparison of ISI histograms across many recordings (**Supplementary Fig. 1**), log-binned ISI histograms for each cell were normalized to the maximum number of intervals measured in any bin.

*Mini-burst distribution within bursts*. To characterize the progressive shortening and lengthening of intervals separating mini-bursts at the onset and end of each burst, a custom routine was written in Igor 6.0 to identify and number successive inter-mini-burst intervals within bursts in each recording using boundary values obtained with the $CV_b$ analysis. We limited our analysis to bursts composed of a minimum of 10 mini-burst intervals and to recordings containing at least 5 such bursts. For each cell, the first and last 5 mini-burst intervals of each burst were aligned to the beginning and end of each burst, respectively and the mean duration of mini-burst intervals at each position was calculated.

**Supplementary Discussion**

Comparison of the spontaneous activity of auditory neurons in the brain and the cochlea indicate that immature auditory circuits have a remarkable ability to preserve the overall discharge patterns imposed by IHCs. Although there have been few physiological studies of these developing circuits, anatomical studies in adult cats indicate that globular bushy cells (GBCs), which innervate MNTB neurons with a single, giant axo-somatic terminal known as the calyx of Held[4] receive dozens of converging auditory nerve inputs (5 to 69, mean = 23)[5,6]. If a similar convergence exists during the prehearing period, it would likely disrupt IHC-generated activity patterns unless inputs to GBCs fire synchronously or there is one dominant suprathreshold input. Although the degree of 8$^{th}$ nerve convergence has not been determined in rodents before the onset of hearing, it appears to be much smaller in adult mice (4 to 7)[7] than in cats, and physiological studies of bushy cells in the ventral division of cochlear nucleus do not distinguish between spherical and globular bushy cells[8,9], suggesting that both cell types may receive one dominant input. Moreover, there is evidence that multiple synaptic endings on GBCs can originate from the same branched auditory nerve fiber[6,10]. The disruptive effect of convergence would be further reduced if the SGNs that project to each GBC receive inputs from the same IHC (as each IHC is innervated by as many as 30 SGNs). Further experiments will be required to determine the extent of convergence onto GBCs before the onset of hearing.

Despite the remarkable similarity in discharge patterns exhibited by SGNs *in vitro* and central auditory neurons *in vivo*, some notable differences exist. In particular, discharge patterns in MNTB and CIC neurons *in vivo* were often more similar to the activity of SGNs recorded at room temperature than at near-physiological temperatures; mean firing rates were significantly higher and intervals separating action potentials within mini-bursts were considerably shorter in SGNs at physiological temperature compared to MNTB and CIC neurons. It is possible that these differences arise from the properties of intervening synapses in the developing cochlear nucleus or superior olivary complex. It is also possible that these differences are simply due to technical limitations that arise from comparing activity between *in vivo* and *ex vivo* preparations. Specifically, *in vivo* recordings were performed in the presence of anesthetics, which can affect

excitability, firing rates and synaptic release probabilities. In addition, the organ of Corti normally exists within a privileged environment – exposed on one side to high potassium containing endolymph, and on the other to perilymph – that cannot be mimicked *in vitro*. Studies in isolated cochleae are typically performed in extracellular saline enriched in potassium (5–6 mM), although it is unclear whether this condition mimics the endogenous environment of IHCs in the neonatal cochlea.

In addition, some differences were apparent between the discharge patterns of MNTB and CIC neurons recorded under similar conditions *in vivo*: CIC neurons fired bursts that were shorter in duration and contained fewer action potentials, and intervals separating action potentials within mini-bursts also appeared longer. These discrepancies presumably arise from the anatomical and functional differences between these auditory centers. While principal neurons in the MNTB are part of a pathway specialized for preserving auditory nerve input patterns from one ear[4], CIC is a major relay nucleus that integrates ascending excitatory and inhibitory inputs from more than ten ipsi- and contralateral brainstem auditory nuclei, as well as descending modulatory projections from auditory cortex[11]. The complex intervening circuitry between the cochlea and CIC, as well as inhibitory networks within the CIC, may both limit the propagation of burst activity and shape the timing of action potentials within each burst. It will be important to determine which elements in these developing circuits modify propagation of cochlea-initiated patterns during the pre-hearing period.

**Supplementary References**


1. Tritsch, N.X., Yi, E., Gale, J.E., Glowatzki, E. & Bergles, D.E. *Nature* **450**, 50-55 (2007).
2. Tritsch, N.X. & Bergles, D.E. *J Neurosci* **30**, 1539-1550 (2010).
3. Rodriguez-Contreras, A., van Hoeve, J.S., Habets, R.L.P., Locher, H. & Borst, J.G.G. *Proc Natl Acad Sci U S A* **105**, 5603-5608 (2008).
4. von Gersdorff, H. & Borst, J.G.G. *Nat Rev Neurosci* **3**, 53-64 (2002).
5. Spirou, G.A., Rager, J. & Manis, P.B. *Neuroscience* **136**, 843-863 (2005).
6. Liberman, M.C. *J Comp Neurol* **313**, 240-258 (1991).
7. Oertel, D. *J Acoust Soc Am* **78**, 328-333 (1985).
8. Isaacson, J.S. & Walmsley, B. *J Neurophysiol* **73**, 964-973 (1995).
9. Oleskevich, S., Clements, J. & Walmsley, B. *J Physiol* **524 Pt 2**, 513-523 (2000).
10. Rouiller, E.M., Cronin-Schreiber, R., Fekete, D.M. & Ryugo, D.K. *J Comp Neurol* **249**, 261-278 (1986).
11. Malmierca, M.S. *Neuroembryol Aging* **3**, 215-229 (2004).
12. Elgoyhen, A.B., Johnson, D.S., Boulter, J., Vetter, D.E. & Heinemann, S. *Cell* **79**, 705-715 (1994).

**Supplementary Figures**

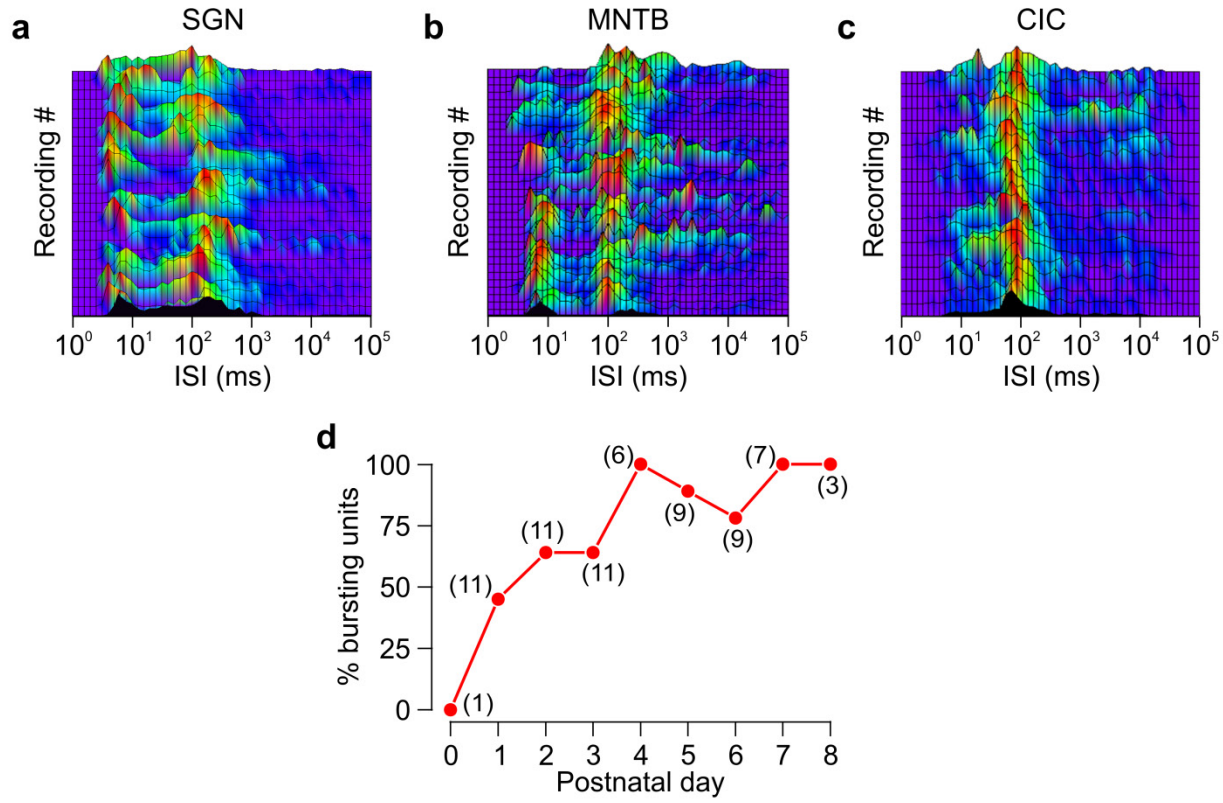


**Supplementary Figure 1** Firing patterns of SGNs *in vitro*, and MNTB and CIC neurons *in vivo*, before the onset of hearing. (**a**) Normalized log-binned ISI frequency distributions of action potentials recorded from 27 SGNs (distributed along the ordinate) in prehearing cochlear explants at room temperature. Warmer colors indicate more frequently observed intervals. (**b**,**c**) Normalized log-binned ISI frequency distributions of action potentials recorded from 34 MNTB neurons in P4–8 rats (**b**) and 21 CIC neurons at P4–7 (**c**). (**d**) Percentage of all MNTB units displaying burst firing *in vivo* as a function of postnatal age (in days). Number of recordings indicated in parentheses.

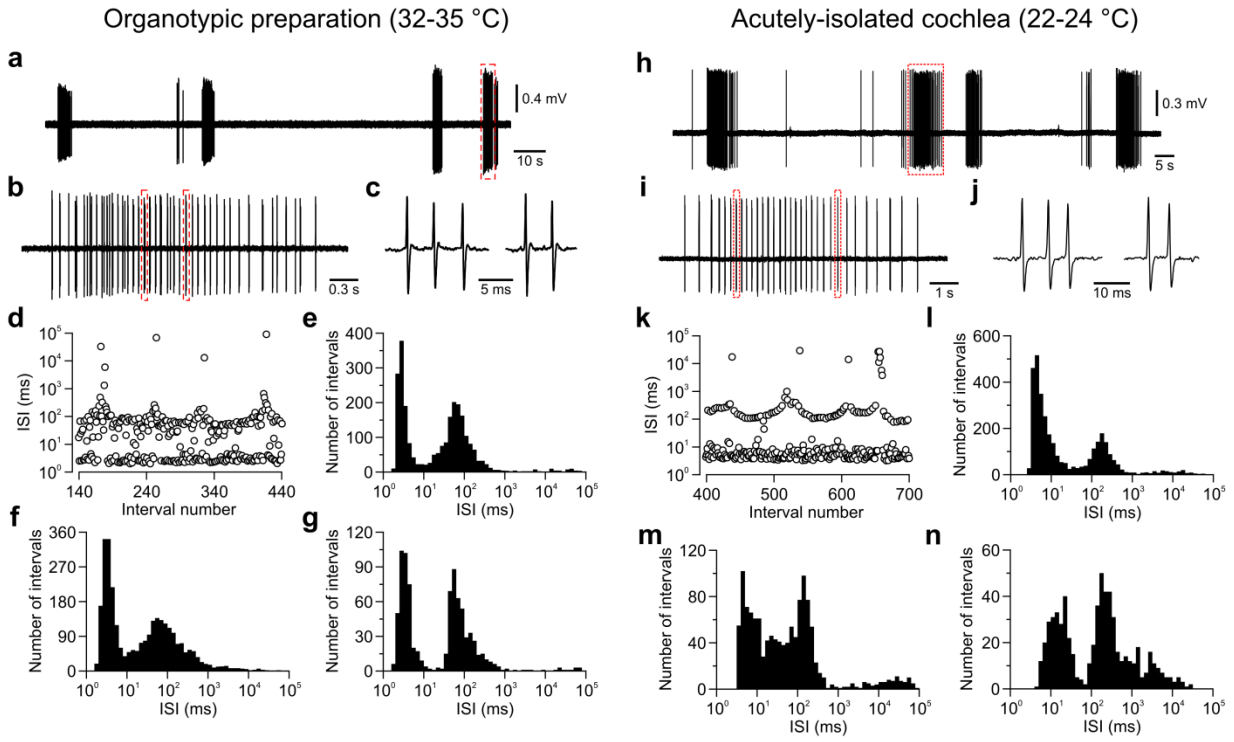


**Supplementary Figure 2** SGNs display similar firing patterns in cochlear explants and in acutely-isolated cochleae. (**a**) Extracellular action potentials recorded from an SGN at 32–35 °C, from a P6 cochlea maintained for 2 days *in vitro*. (**b**) Burst within dashed red box in **a** shown on expanded time scale. (**c**) Detail of two mini-bursts within dashed red boxes in **b**. (**d**,**e**) Plot of 300 consecutive ISI intervals (log scale, **d**) and log-binned ISI histogram (**e**) for the cell in **a**. (**f**,**g**) Log-binned ISI histograms for two additional extracellular SGN recordings performed at 32–35 °C. (**h**–**l**) Same as in (**a**–**e**) for a SGN recorded at room temperature in a cochlea acutely isolated from a P9 rat. (**m**,**n**) Log-binned ISI histograms for another P9 (**m**) and a P5 (**n**) SGN in acutely-isolated cochleae at room temperature. P5 recordings were performed in extracellular solution containing 2.5 mM $K^+$; all other recordings were performed in extracellular solution containing 6 mM $K^+$.

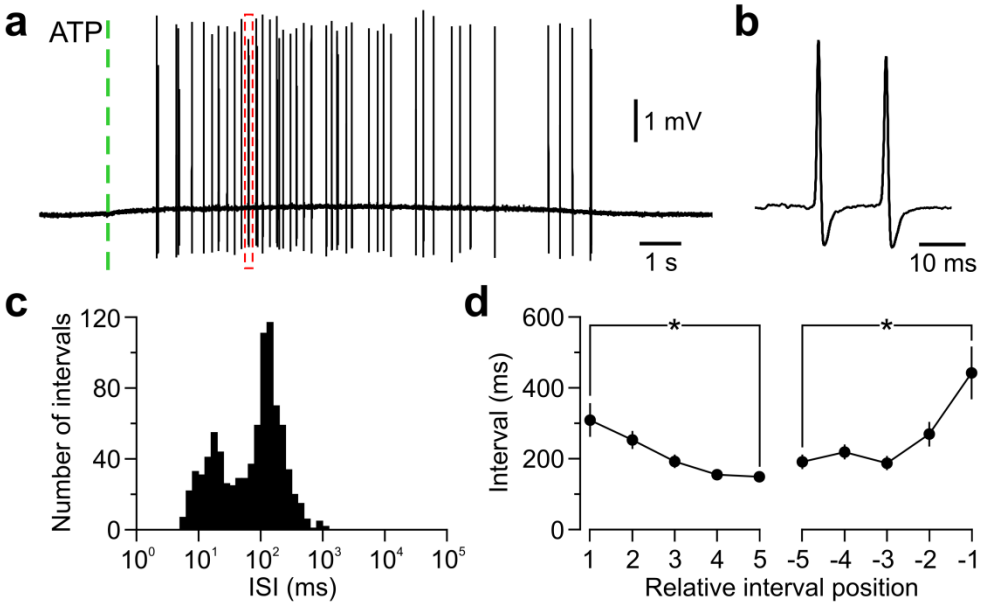


**Supplementary Figure 3** Stimulation of an IHC with ATP triggers a train of action potential mini-bursts in the postsynaptic SGN. (**a**) Extracellular action potentials recorded from an SGN in response to application of ATP (10 μM, 50 ms, 5 psi; dashed green line) to its presynaptic IHC. (**b**) Detail of a mini-burst outlined by the dashed red box in **a**. (**c**) Log-binned histogram of all SGN action potentials evoked in response to ATP (10 μM) application ($n$ = 900 action potentials in 5 SGNs). (**d**) Mean duration (± s.e.m.) of intervals separating mini-bursts vs. relative mini-burst position within a burst ($n$ = 19 bursts in 5 SGNs). * $P < 0.005$, paired t-test. Recordings in **a**–**d** were performed in the presence of strychnine (1 μM), an α9/α10 acetylcholine receptor antagonist[12], indicating that efferent input to prehearing IHCs is not required to initiate patterned bursts of action potentials in SGNs.

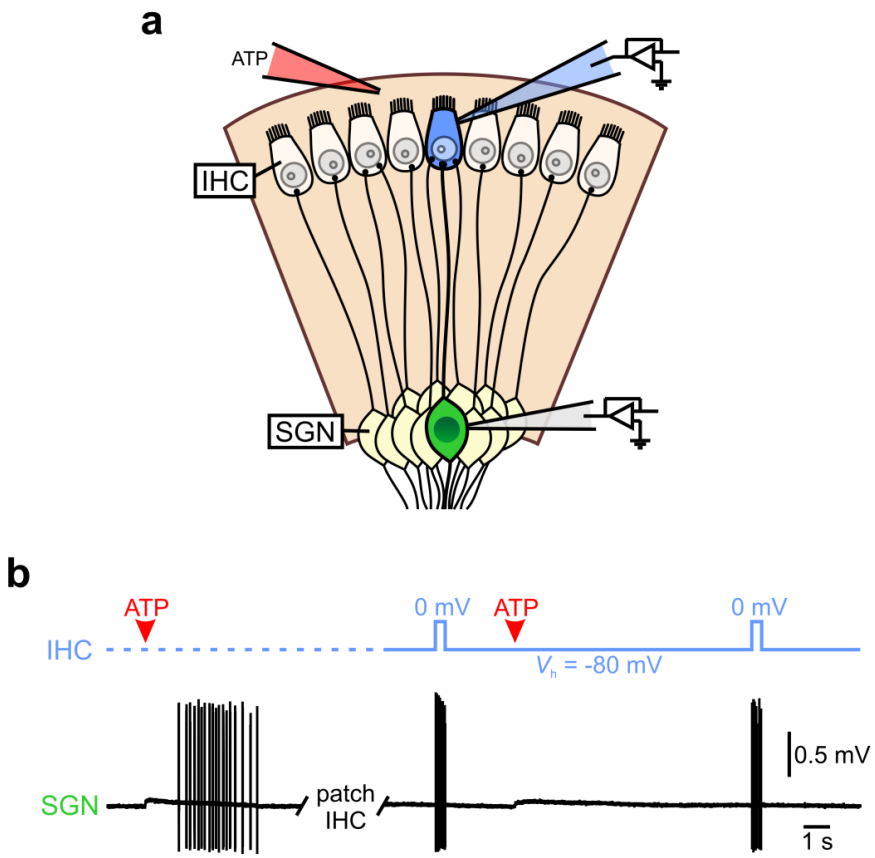


**Supplementary Figure 4** Sequence used to identify SGNs that receive input from a single IHC. (**a**) Diagram of the paired IHC-SGN recording configuration in an organotypic preparation. Once a stable extracellular recording was established from a SGN (labeled in green), we identified the region in the organ of Corti innervated by this neuron using small ATP puffs (10–100 μM, 5 psi; red pipette) delivered to IHCs. Upon identification of the presynaptic region, several IHCs were patched until the presynaptic cell (indicated in blue) was found. (**b**) Representative recording illustrating the protocol employed to ensure that each SGN only received synaptic inputs from a single IHC. *Top*. Command voltage ($V_h$) applied to the presynaptic IHC. Dashed line indicates time period prior to obtaining whole-cell recording from the presynaptic IHC. *Bottom*. Extracellular recording from a SGN (obtained first). The small positive deflections induced by ATP application to IHCs represent source waves resulting from inward currents in supporting cells[1]. Depolarization of the presynaptic IHC to 0 mV triggered a burst of action potentials in the recorded SGN, but exogenous ATP (red arrowheads) was unable to elicit a burst of action potentials when the presynaptic IHC was voltage-clamped at –80 mV, indicating that this SGN did not receive synaptic inputs from surroundings IHCs.

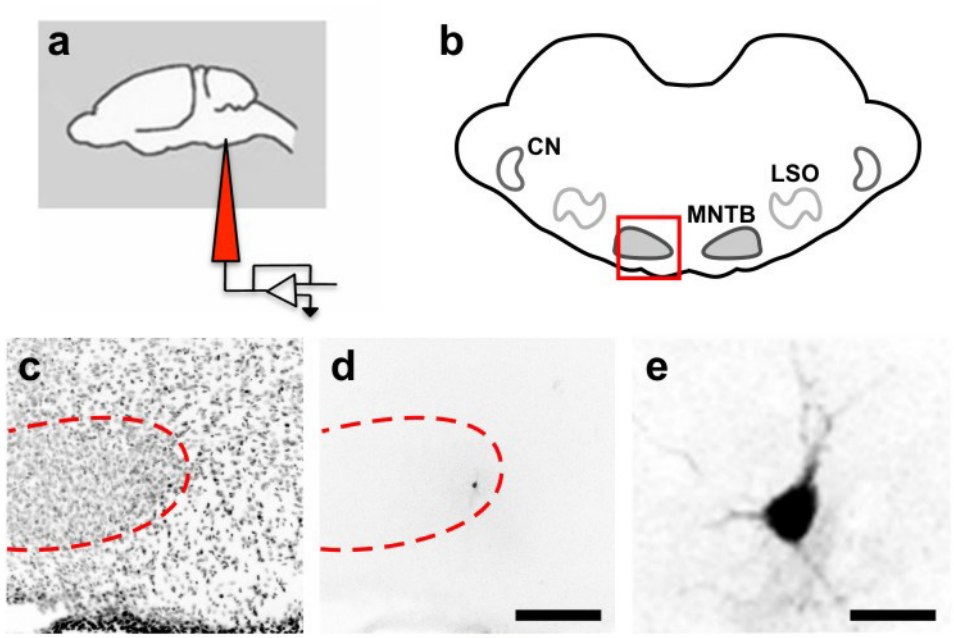


**Supplementary Figure 5** Morphological and anatomical identification of MNTB neurons recorded from *in vivo*. (**a**) Experimental configuration. A patch electrode filled with a fluorescent dye was advanced into the ventral side of the brainstem according to anatomical landmarks and a whole-cell (not in this paper) or extracellular recording was obtained. After perfusion fixation, coronal 50 µm thick brain sections were obtained, the tissue was counterstained with DAPI and then mounted onto coverslides. (**b**) Schematic of the cochlear nucleus (CN), MNTB and lateral superior olive (LSO) in a coronal brainstem slice. Red box indicates the area shown in panels **c** and **d**. (**c**) Example of a DAPI counterstained P1 brain section at the level of the MNTB (circled by dashed red line). (**d**) Same region as in **c** indicating the position of the Alexa594-filled principal cell. MNTB outline is indicated by dashed red line. Scale bar: 200 µm. (**e**) Higher magnification view of the dye-filled principal neuron shown in panel **d**. Scale bar: 15 µm.

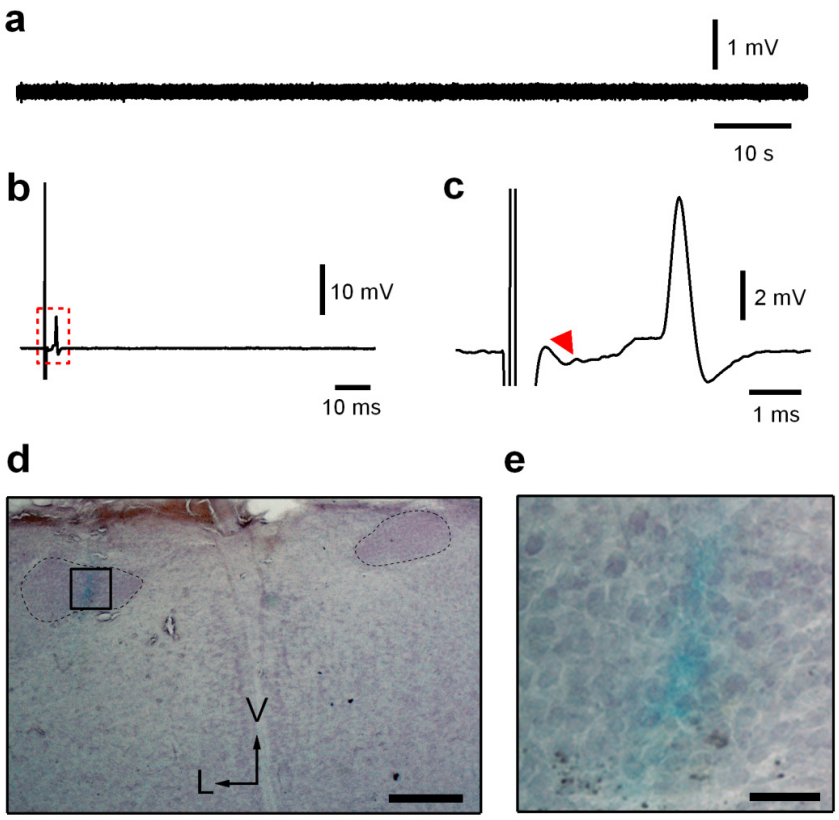


**Supplementary Figure 6** Cochlear ablation silences MNTB neurons *in vivo*. (**a**) Continuous recording from a unit in a P5 animal following ablation of the contralateral cochlea. No action potentials were observed in 68 extracellular recordings from putative MNTB principal neurons in six animals (> 6 units/animal); in each animal bursting activity from a unit with a complex waveform was recorded before ablation. A single bursting unit was observed in each of two additional animals; however, after further cochlear dissection, all MNTB neurons (15 units/animal) were silent in these rats, suggesting that the cochlea had been incompletely ablated. (**b**) Response of a unit in the same animal shown in **a** to afferent stimulation at the midline after cochlea ablation. The complex waveform indicates that this was an MNTB principal neuron. Stimulus artifact is partially truncated. Note the lack of spontaneous activity preceding and following the electrically-evoked complex waveform. Similar results were obtained in a total of six units from four different animals. (**c**) Enlargement of the boxed area in **b**. The red arrowhead marks the pre-spike. (**d**) Section containing the ventral brainstem showing the presence of blue dye within the MNTB (outlined with dashed black line) injected at the same site as units illustrated in **a–c**. Scale bar: 200 µm. L, lateral; V, ventral. Vertical arrow indicates the midline. (**e**) Magnification of boxed area shown in **d**. Scale bar: 50 µm.

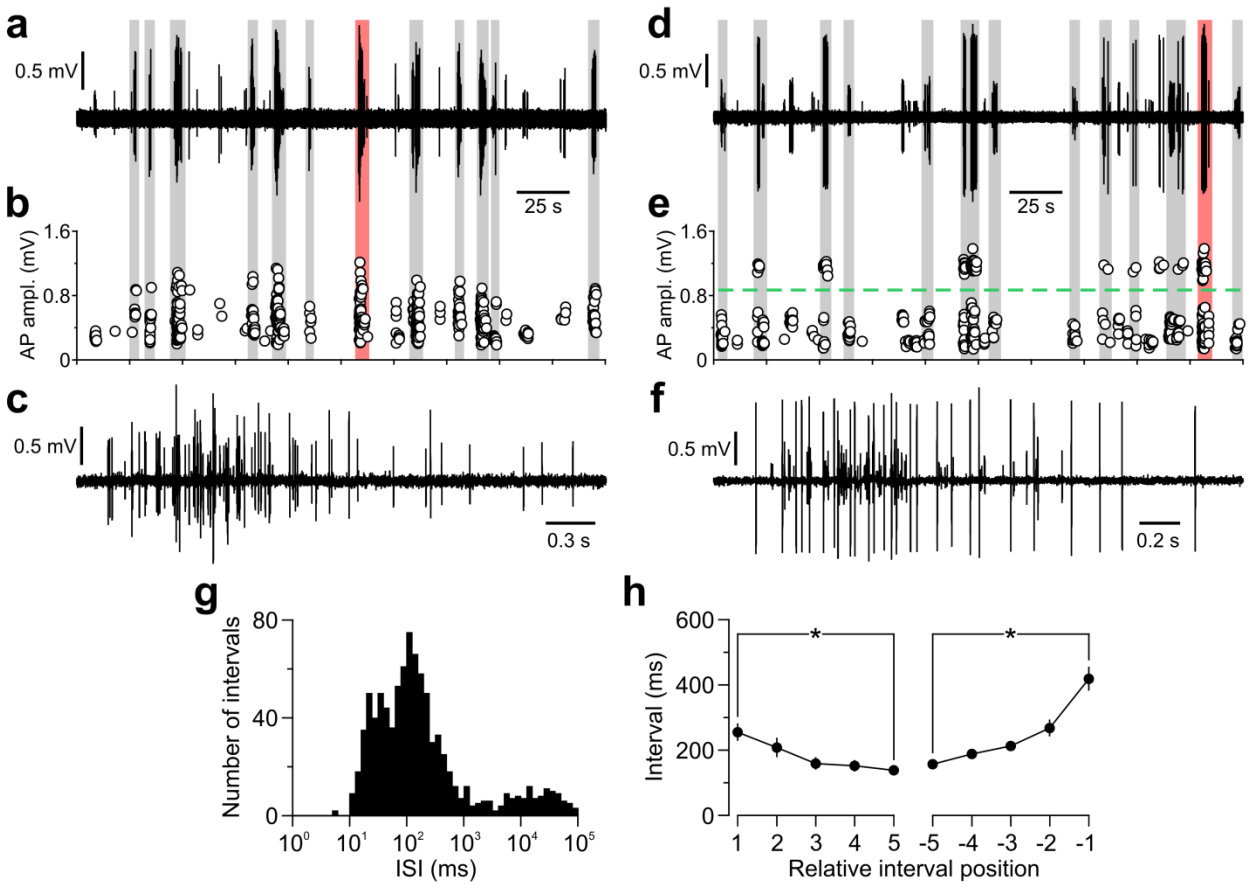


**Supplementary Figure 7** CIC neurons fire correlated bursts of patterned action potentials before hearing onset. (**a**) *In vivo* multi-unit extracellular recording from CIC in a P5 pup. (**b**) Scatter plot of peak action potential amplitude vs. spike time for the recording shown in **a**. Bursts (highlighted in gray) are composed of action potentials with widely varying amplitudes, indicating coincident discharge of groups of neighboring neurons. (**c**) Detail of the multi-unit burst highlighted in red in **a**. (**d–f**) Same as **a–c** for another recording obtained in a P7 animal. Note in **e** that one unit is clearly distinguishable from others (dashed green line), offering the possibility to define its pattern. (**g**) Log-binned ISI histograms for the largest unit in **d**. (**h**) Mean duration (± s.e.m.) of mini-burst intervals within bursts ($n$ = 110 bursts in 9 units). * $P < 0.005$, paired t-test.

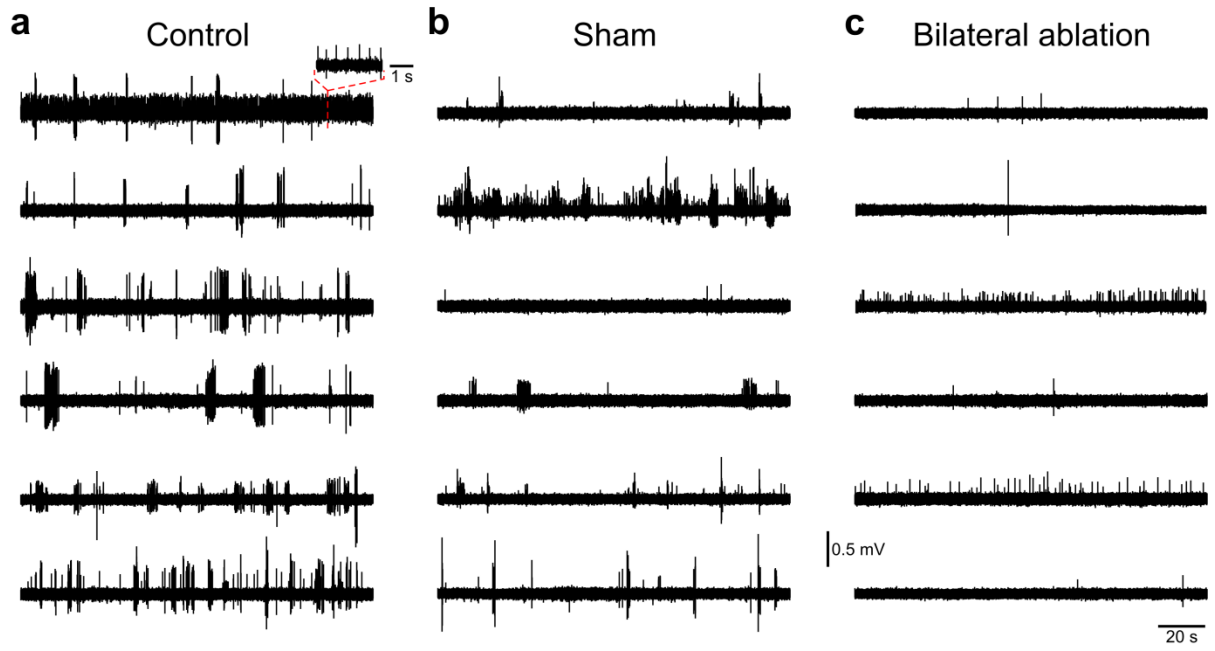


**Supplementary Figure 8** Spontaneous correlated bursts of action potentials in CIC originate in the cochlea. (**a–c**) Spontaneous multi-unit activity recorded in CIC from six control (**a**), sham-operated (**b**) or ablated (**c**) animals (P4–7). Spontaneous bursting activity was recorded from most electrode tracks in which action potentials were detected in control ($n$ = 36/43, 84 % in 13 pups) and sham-operated animals ($n$ = 8/11, 73% of electrode tracks in 6 pups), but was never observed in animals in which both cochleae had been removed ($n$ = 0/20 electrode tracks in which action potentials were detected in 7 pups). Recordings with sparse activity or regularly-discharging units were observed in all animals, indicating that the source of this activity is extrinsic to the cochlea.